doi:10.1016/j.jmb.2007.08.057 J. Mol. Biol. (2007) 373, 1269–1280

JMB

Available online at www.sciencedirect.com

ScienceDirect

ELSEVIER

Ligand-induced Conformational Changes *via* Flexible Linkers in the Amino-terminal region of the Inositol 1,4,5-Trisphosphate Receptor

Jenny Chan[1], Andrew E. Whitten[2,3], Cy M. Jeffries[3], Ivan Bosanac[1] Tapas K. Mal[1], Jennifer Ito[1], Horea Porumb[4], Takayuki Michikawa[5,6,7] Katsuhiko Mikoshiba[5,6,7], Jill Trewhella[3]* and Mitsuhiko Ikura[1]*

[1]*Division of Signaling Biology Ontario Cancer Institute Department of Medical Biophysics, University of Toronto, Toronto, ON Canada M5G 1L7*

[2]*Bragg Institute, Australian Nuclear Science and Technology Organization, Lucas Heights NSW 2234, Australia*

[3]*School of Molecular and Microbial Biosciences, University of Sydney, NSW 2006 Australia*

[4]*Unité de Biochimie Enzymologie - Physicochimie et Pharmacologie des Macromolécules Biologiques UMR CNRS 8113, Institut "Gustave Roussy", 94805 Villejuif Cedex, France*

[5]*Division of Molecular Neurobiology, Department of Basic Medical Sciences The Institute of Medical Science The University of Tokyo Tokyo 108-8639, Japan*

[6]*Laboratory for Developmental Neurobiology, Brain Science Institute, RIKEN, Saitama 351-0198, Japan*

[7]*Calcium Oscillation Project International Cooperative Research Project-Solution Oriented Research for Science*

Cytoplasmic Ca^{2+} signals are highly regulated by various ion transporters, including the inositol 1,4,5-trisphosphate (IP_3) receptor (IP_3R), which functions as a Ca^{2+} release channel on the endoplasmic reticulum membrane. Crystal structures of the two N-terminal regulatory regions from type 1 IP_3R have been reported; those of the IP_3-binding core (IP_3R_{CORE}) with bound IP_3, and the suppressor domain. This study examines the structural effects of ligand binding on an IP_3R construct, designated IP_3R_N, that contains both the IP_3-binding core and the suppressor domain. Our circular dichroism results reveal that the IP_3-bound and IP_3-free states have similar secondary structure content, consistent with preservation of the overall fold within the individual domains. Thermal denaturation data show that, while IP_3 has a large effect on the stability of IP_3R_{CORE}, it has little effect on IP_3R_N, indicating that the suppressor domain is critical to the stability of IP_3R_N. The NMR data for IP_3R_N provide evidence for chemical exchange, which may be due to protein conformational dynamics in both apo and IP_3-bound states: a conclusion supported by the small-angle X-ray scattering data. Further, the scattering data show that IP_3R_N undergoes a change in average conformation in response to IP_3 binding and the presence of Ca^{2+} in the solution. Taken together, these data lead us to propose that there are two flexible linkers in the N-terminal region of IP_3R that join stably folded domains and give rise to an equilibrium mixture of conformational sub-states containing compact and more extended structures. IP_3 binding drives the conformational equilibrium toward more compact structures, while the presence of Ca^{2+} drives it to a more extended set.

**Corresponding authors.* E-mail addresses: jtrewhella@usyd.edu.au; mikura@uhnres.utoronto.ca.

Abbreviations used: IP_3R, inositol 1,4,5-trisphosphate receptor; IP_3R1, type 1 IP_3R; IP_3R2, type 2 IP_3R; IP_3R3, type 3 IP_3R; mIP_3R1, mouse type 1 IP_3R; IP_3R_N, residues 1–604 of mIP_3R1; IP_3R_{CORE}, residues 224–604 of mIP_3R1; IP_3, D-myo-inositol 1,4,5-trisphosphate; HSQC, heteronuclear single quantum coherence; SAXS, small-angle X-ray scattering; MS, mass spectrometry; TCEP, Tris(2-carboxyethyl)phosphine hydrochloride; DLS, dynamic light-scattering.

0022-2836/$ - see front matter © 2007 Published by Elsevier Ltd.

and Technology, Japan Science and Technology Agency Saitama 332-0012, Japan

Received 14 June 2007; received in revised form 24 August 2007; accepted 24 August 2007
Available online 29 August 2007

Edited by M. F. Summers

Keywords: circular dichroism; NMR; small-angle X-ray scattering; modeling; conformational variability

Introduction

Calcium signaling is involved in a variety of physiological processes, including fertilization, muscle contraction, vision, memory, and learning.[1] In electrochemically non-excitable tissues, complex Ca^{2+} signals are generated by inositol 1,4,5-trisphosphate (IP_3) receptors (IP_3Rs). The IP_3Rs are intracellular Ca^{2+} release channels that are conserved from *Caenorhabditis elegans* to humans.[1] In mammals, three isoforms (IP_3R1, IP_3R2, and IP_3R3) have been identified that are expressed differentially across tissue types.[2] Binding of IP_3 to IP_3R in the presence of ~1 μM cytosolic Ca^{2+} induces channel opening and the mobilization of Ca^{2+} from stores such as the endoplasmic reticulum (ER).[3]

The 2749 residue mouse IP_3R1 polypeptide consists of three regions; an N-terminal ligand-binding region, a central regulatory region, and a C-terminal channel region that contains six putative transmembrane helices and an ion-conducting pore that is believed to be located between transmembrane helices 5 and 6.[4,5] The N-terminal region, IP_3R_N, is composed of the so-called suppressor domain (amino acid residues 1–225 of mIP_3R1) and the IP_3-binding core (residues 226–604). The presence of the suppressor domain decreases the IP_3-binding affinity by more than tenfold in the 734 N-terminal residues,[6,7] and has been shown to have a crucial role in coupling ligand binding to channel opening, as its deletion results in a non-functional channel in spite of the augmented affinity for IP_3.[8]

Several groups have studied the overall structure of IP_3R by electron microscopy,[9–14] and we determined the crystal structures of the IP_3R1 suppressor domain[15] and the IP_3-binding core.[16] The suppressor domain contains a modified β-trefoil fold (βI) and the IP_3-binding core contains a β-trefoil domain (βII) with an additional C-terminal domain that has an armadillo-like repeat fold (ARM). IP_3 binds to a positively-charged pocket at the interface of the βII and ARM domains, and is coordinated by residues from both domains. There is no crystal structure available for the intact IP_3R_N, and so how the different functional domains interact is unknown. Previous mutagenesis studies provided clues to the determinants of IP_3-binding inhibition but the precise mechanism by which the suppressor domain influences IP_3-binding and the nature of the conformational changes triggered by IP_3 binding are unknown.[15] To investigate domain interactions and the effects of IP_3 binding on IP_3R_N, we employed a variety of biophysical methods. Small-angle X-ray scattering (SAXS) in combination with circular dichroism (CD) and NMR data provide evidence for ligand-induced structural changes and conformational flexibility within this key regulatory region.

Results

The N-terminal region of IP_3R is folded even in the IP_3-free form

To address the question of whether the suppressor domain and IP_3-binding core are structured in the absence of IP_3, and what effects IP_3 binding has on the overall domain architecture, we utilized two protein constructs; one encompassing only the IP_3-binding core, IP_3R_{CORE} (residues 224–604 of mIP_3R1), the other containing both the suppressor domain and the IP_3-binding core, IP_3R_N (residues 1–604 of mIP_3R1) (Figure 1). We first acquired far-UV CD spectra for IP_3R_{CORE} and IP_3R_N, with and without IP_3 bound (Figure 2(a) and (b)). The CD data indicate that the IP_3-bound IP_3R_{CORE} contains a mixture of α-helical and β-strand. This mixture is consistent with its crystal structure, and is not significantly altered upon removal of IP_3. A slightly more intense signal is observed for the IP_3-bound IP_3R_{CORE} at ~210–220 nm (Figure 2(b)), which may signify an IP_3-induced rigidity of the overall structure. In the case of IP_3R_N, the spectra of IP_3-free and IP_3-bound states are identical, indicating that the three structural domains in the N-terminal region (βI, βII, and ARM) are folded before IP_3 binding.

To further investigate the effects of IP_3 on the domain architecture of IP_3R_N, the protein was subjected to limited trypsin digestion. Trypsinization of IP_3R_N in the absence (Figure 2(c)) or in the presence of IP_3 (Figure 2(d)) resulted in a similar pattern of proteolytic fragments. In both cases, two major products were observed with molecular mass of ~40 kDa and ~31 kDa. The matrix-assisted laser

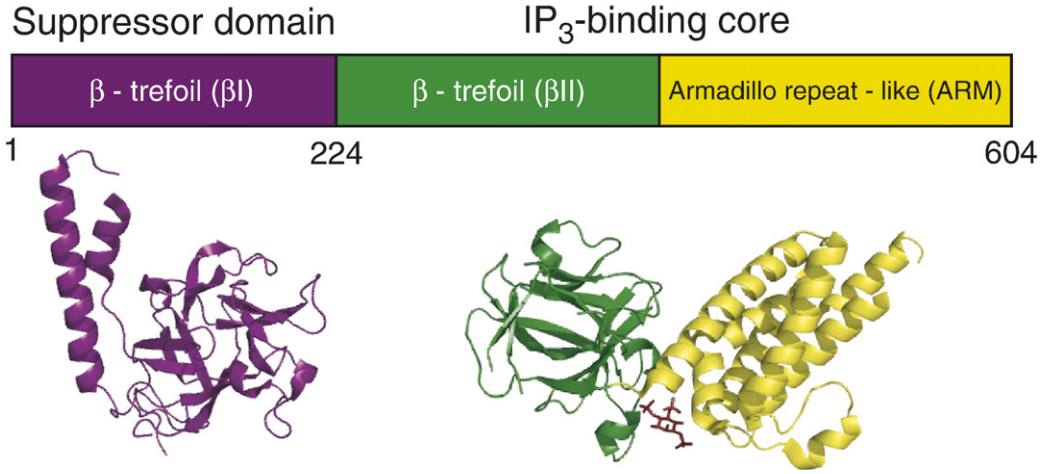

Figure 1. Schematic of the N-terminal region of IP_3R_1. The IP_3R_N (mouse IP_3R_1 residues 1–604) protein construct contains both the suppressor domain (residues 1–223), and the IP_3-binding core, IP_3R_{CORE} (residues 224–604). The crystal structures of the suppressor domain and the IP_3-bound core are depicted as ribbon diagrams.

desorption/ionization-time of flight (MALDI-TOF) mass spectrometry data indicate that these fragments are produced by cleavage of the protein at a site in the unstructured region (residues 320–350) between β-strands 6 and 7 in the β-trefoil domain of the IP_3R_{CORE} (data not shown). These results demonstrate that IP_3 binding does not impact the accessibility of the proteolytic site found in this loop within the IP_3-binding core, and are consistent with the idea that the domain folds observed in the structures of the IP_3-loaded IP_3R_{CORE} and the suppressor domain, are maintained in the absence of IP_3.

Interdomain interactions are suggested by thermal denaturation

We next investigated the stabilities of the protein constructs and asked whether the three structural

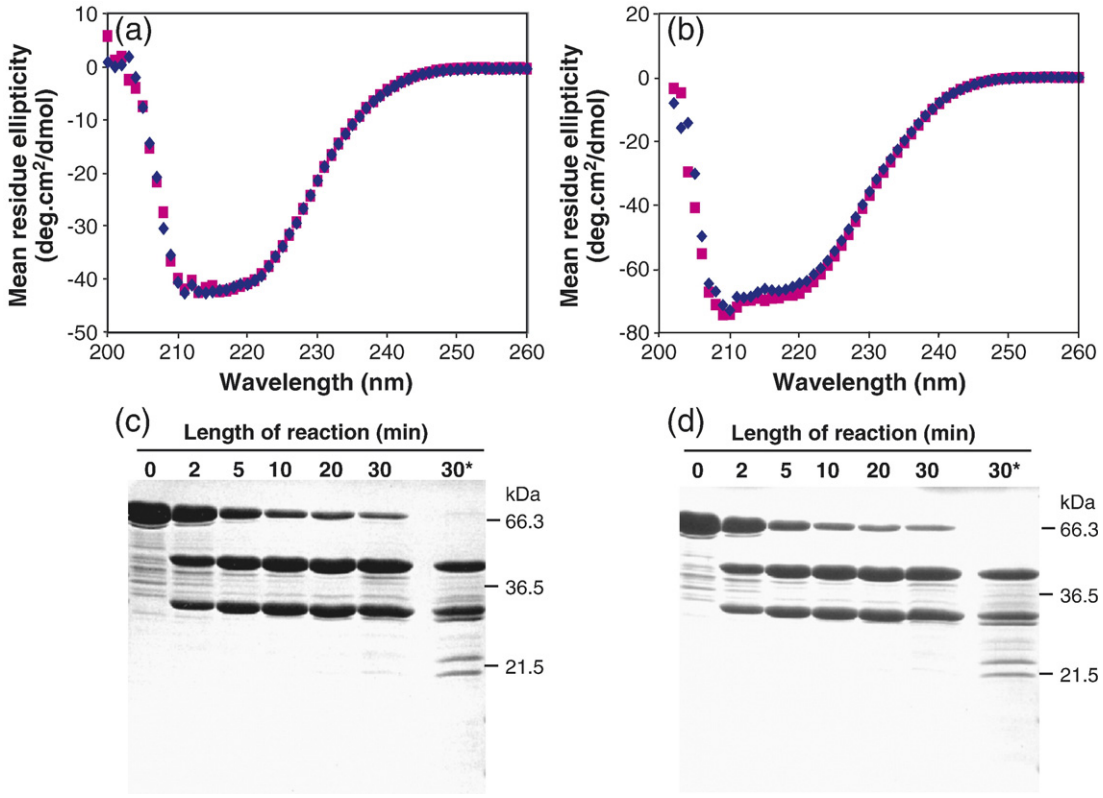

Figure 2. Far-UV CD analysis of IP_3R_N and IP_3R_{CORE} and SDS-PAGE analysis of limited trypsin proteolysis of IP_3R_N. CD spectra of (a) IP_3R_N and (b) IP_3R_{CORE} in the presence (pink squares) and in the absence (blue diamonds) of IP_3. (c) Purified IP_3-free and (d) IP_3-bound IP_3R_N were subjected to digestion by 0.2 μg/ml trypsin for 0, 2 min, 5 min, 10 min, 20 min, and 30 min at 37 °C. Asterisks denote samples digested by trypsin at 2 μg/ml for 30 min at 37 °C.

domains behave independently or in a coupled manner in contributing to the structural integrity of the N-terminal region. To determine the thermal stabilities of IP_3R_{CORE} and IP_3R_N, we monitored the CD ellipticity at 222 nm at various temperatures. The thermal melting data of both protein constructs show sigmoidal curves with a single transition point (Figure 3(a) and (b)), indicating that the proteins unfold in a highly cooperative manner. The high level of cooperativity observed in the melting curves suggests that the three structural domains in both the IP_3-free and IP_3-bound states behave as one structural entity, and that their unfolding is highly interdomain-dependent. It should be noted that the thermal denaturation was irreversible, causing the proteins to precipitate, thus preventing further analysis of the thermodynamic process.

For IP_3R_{CORE}, the apparent melting temperature (T_m) of the IP_3-bound form is significantly higher (~55 °C) than that of the IP_3-free form (~45 °C) (Figure 3(b)). On the other hand, the IP_3-bound form of IP_3R_N displayed only a slight increase in its apparent T_m as compared to the IP_3-free form (from ~51 °C to 53 °C) (Figure 3(a)). Evidently, the suppressor domain stabilizes the N-terminal region of IP_3R_N but, in the absence of the suppressor domain, stabilization is imparted by IP_3-binding. These results suggest strongly that interdomain interactions between βI and βII and/or ARM have a crucial role in providing stability to the protein.

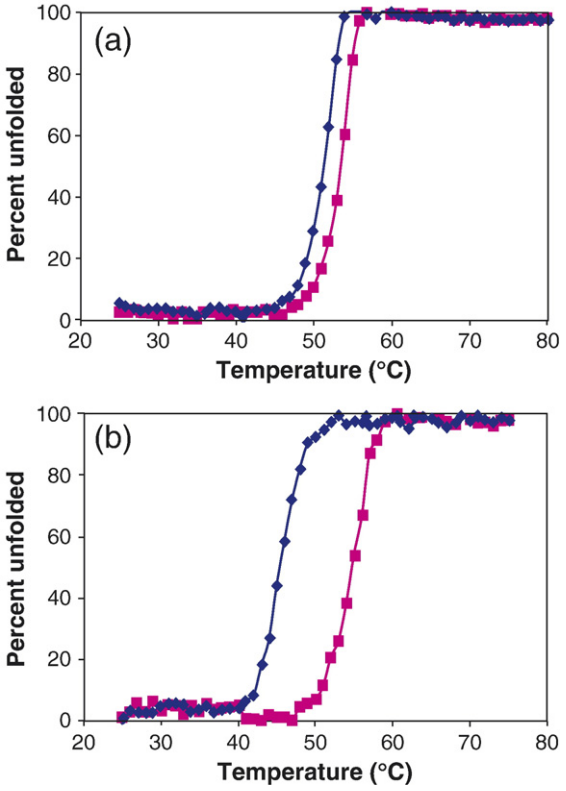

Figure 3. Protein stabilities of IP_3R_N and IP_3R_{CORE}. Relative thermal stabilities of (a) IP_3R_N and (b) IP_3R_{CORE} as measured by monitoring the molar ellipticity at 222 nm. Conditions without IP_3 are depicted by blue diamonds; pink squares represent conditions with IP_3.

We performed chemical denaturation experiments on IP_3R_N and IP_3R_{CORE} to further probe the effect of IP_3 binding on protein stability. IP_3-induced changes in the protein stabilities were not detected for either construct by monitoring the CD ellipticity at 222 nm in increasing concentrations of guanidine hydrochloride (Supplementary Data Figure 1). This result may be due to the fact that this chemical denaturant, which greatly distorts water structure and consequently alters protein solvation, could inhibit interaction with IP_3, which requires six water molecules in ligand coordination.[16]

NMR evidence for dynamic interdomain interactions

We used NMR spectroscopy in an attempt to gain insight into the nature of the interaction between the suppressor domain and the IP_3-binding core. IP_3-bound IP_3R_{CORE} displayed an excellent ^1H-^{15}N heteronuclear single quantum coherence (HSQC) spectrum (Figure 4(a)) consistent with the well-folded and stable structure of IP_3R_{CORE} in the presence of IP_3. In the absence of IP_3, the quality of the spectrum was reduced dramatically (Figure 4(b)), and we believe the broadening observed in the IP_3-free IP_3R_{CORE} spectrum is due to flexibility and the existence of multiple conformational states. The ^1H-^{15}N HSQC spectrum of the suppressor domain alone (residues 2–223 of mIP_3R1) displayed many peaks dispersed between 6.4 ppm and 10.4 ppm in the ^1H dimension (Figure 4(c)), and is in good agreement with the previously reported crystal structure[15] that contains both β-strands and α-helices. In contrast, the ^1H-^{15}N HSQC spectrum of the IP_3-bound IP_3R_N construct (Figure 4(d)) exhibited severe peak broadening across its entire spectrum, as did the ^1H-^{15}N HSQC spectrum of the IP_3-free IP_3R_N (data not shown). The degree of broadening is beyond that expected for changes in T_2 relaxation resulting from the increase in the size of IP_3R_N compared to the smaller domain constructs. While protein aggregation could give rise to peak broadening, multi-angle light-scattering data on the NMR samples would preclude this as an explanation (Supplementary Data Figure 5). Hence, chemical exchange due to the presence of different conformational sub-states is most likely the cause of the observed peak broadening (see Discussion).

Structural variability probed by SAXS

Changes in inter-domain interactions upon IP_3 binding might give rise to changes in the overall shape of the N-terminal region. We utilized small-angle X-ray scattering (SAXS) to probe possible large-scale ligand-induced conformational changes. Reliable interpretation of SAXS data in terms of protein structure requires that samples contain monodisperse, identical particles. Even small amounts of aggregation will bias the derived

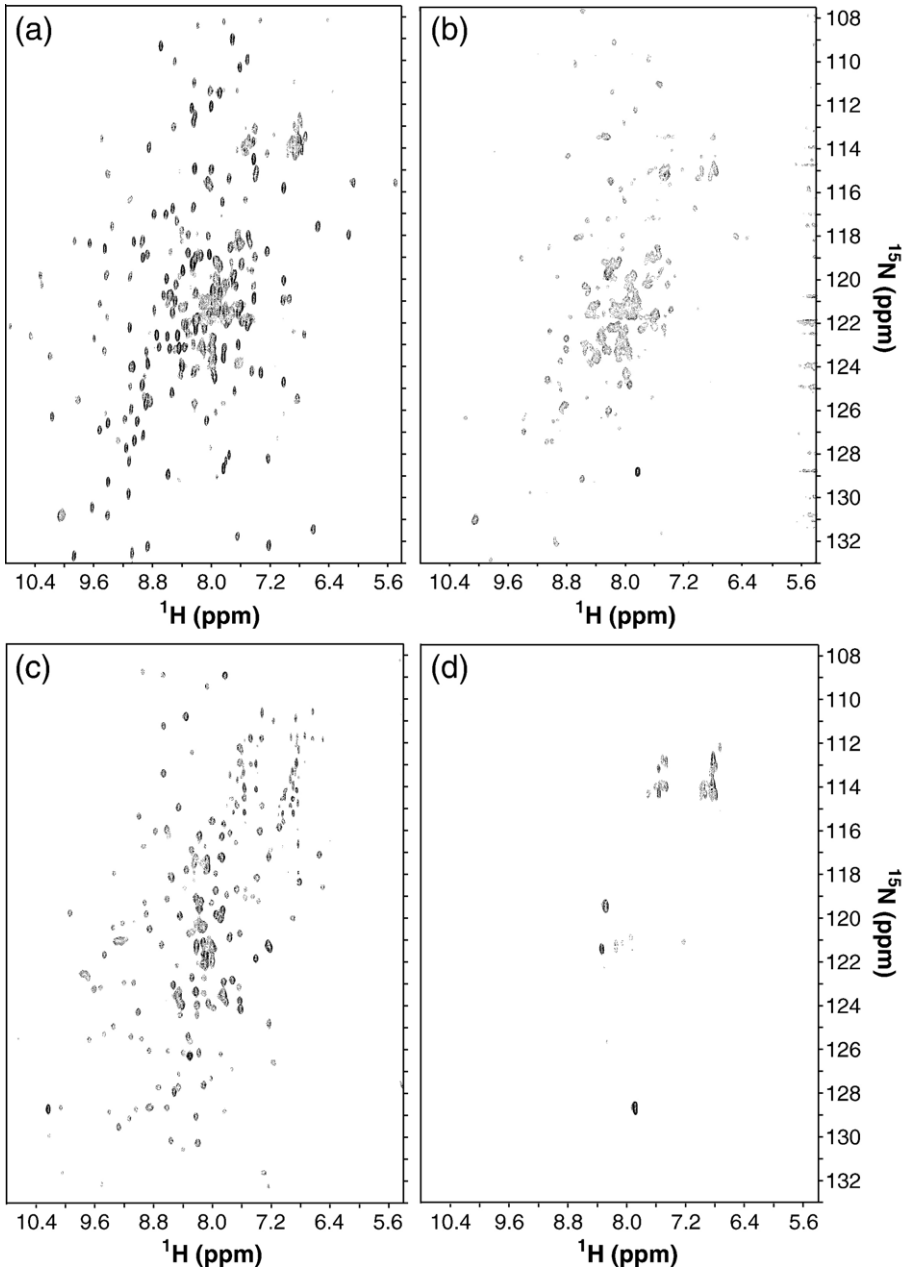

Figure 4. NMR studies of the suppressor domain, IP_3R_{CORE}, and IP_3R_N. ^{15}N-edited HSQC spectra of (a) IP_3-bound IP_3R_{CORE}, (b) IP_3-free IP_3R_{CORE}, (c) the suppressor domain, and (d) IP_3-bound IP_3R_N.

structural parameters. Dynamic light-scattering (DLS) was used to establish the solution conditions for which all four IP_3R_N variants (IP_3R_N, $IP_3R_N + IP_3$, $IP_3R_N + Ca^{2+}$, and $IP_3R_N + Ca^{2+} + IP_3$) are monodisperse. The monodispersity of the four variants at a range of temperatures was also monitored using DLS (Supplementary Data Figure 2), revealing the relative propensity of each towards thermal aggregation. IP_3R_N with bound IP_3 was shown to remain monodisperse at temperatures as high as 35 °C, while removal of IP_3 and addition of Ca^{2+} lowers this temperature significantly, with the order from lowest to highest aggregation temperature being: $IP_3R_N + Ca^{2+} < IP_3R_N < IP_3R_N + Ca^{2+} + IP_3 < IP_3R_N + IP_3$. No data are presented here for the IP_3R_{CORE}, because we were unable to establish solution conditions for the IP_3R_{CORE} that were sufficiently free of aggregation for SAXS experiments.

We performed SAXS measurements (at 20.0 °C) to evaluate the effects of IP_3 and Ca^{2+} on the overall shape of IP_3R_N (Figure 5(a)). While the physiological relevance of Ca^{2+} binding to this region remains unclear, Ca^{2+} proved to be a useful agent for probing flexibility (see Discussion). As expected for samples of monodisperse proteins, the $I(0)$ values determined from the Guinier plots (Figure 5(b)) normalized for protein concentration (in mg/ml) and molecular mass are constant (Table 1). The interatomic distance distribution functions, $P(r)$, were calculated as the inverse Fourier transform of $I(Q)$[17]

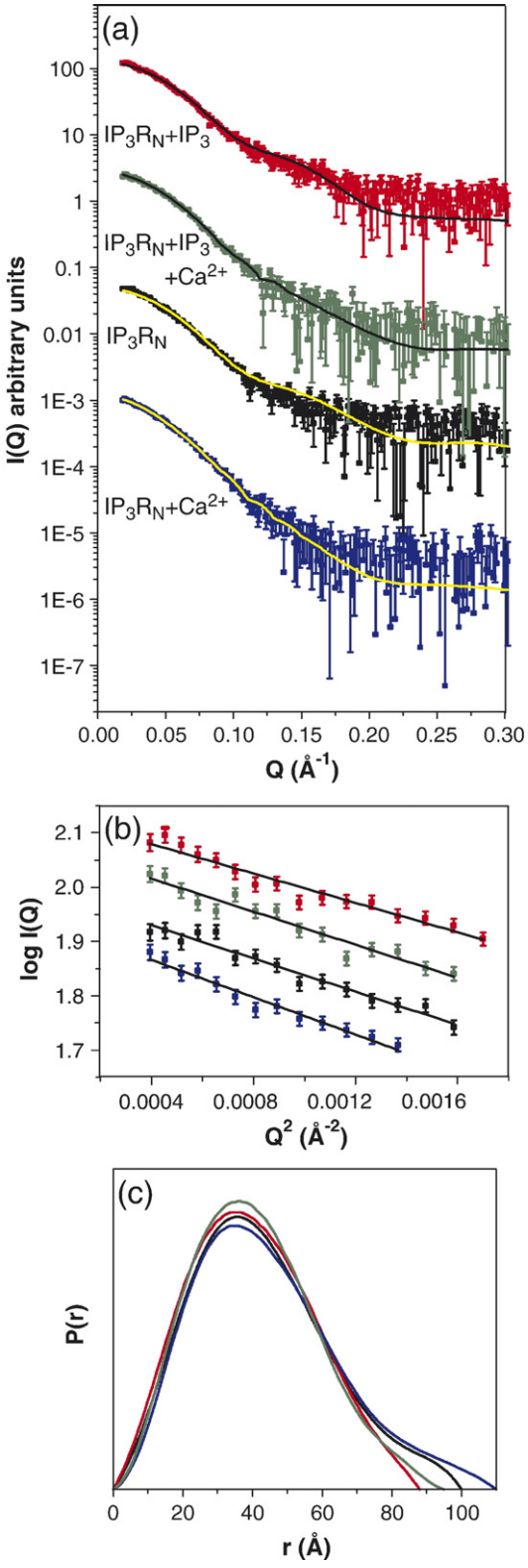

Figure 5. Average global shapes of IP_3R_N and IP_3R_{CORE} in solution. Scattering data as $I(Q)$ *versus* Q, for (a) each of four IP_3R_N variants and (b) Guinier plots for each scattering profile are shown. (c) The $P(r)$ profiles as determined by indirect Fourier transform of the data. The χ^2 values the fits shown in (a) and 1.32 ($IP_3R_N+IP_3$), 1.82 (IP_3R_N), 0.88 ($IP_3R_N+IP_3+Ca^{2+}$) and 0.81 ($IP_3R_N+Ca^{2+}$).

(Figure 5(c)) and the structural parameters determined from the scattering data are summarized in Table 1. The Guinier radius of gyration, R_g, values for IP_3R_N are affected by IP_3 binding and the presence of Ca^{2+}. The smallest R_g value, indicating the most compact structure, is that for IP_3R_N with bound IP_3 and no Ca^{2+} (30.7 Å). Addition of Ca^{2+} or removal of IP_3 results in a significant increase in R_g, with the largest R_g for IP_3R_N with Ca^{2+} and no IP_3 present (34.2 Å). The $P(r)$ profiles and their associated D_{max} values, as well as the volumes determined using the Porod invariant,[18] reflect the same changes in the degree of compaction for each IP_3R_N form. The removal of IP_3 or the presence of Ca^{2+} increases the molecular volume and frequency of larger interatomic distances for IP_3R_N. Again, the largest effects are observed for IP_3R_N with Ca^{2+} and no IP_3 (Porod volume 161,200 Å^3; D_{max} 110 Å). The order of increasing R_g, D_{max} and Porod volumes for each of the four IP_3R_N variants display a negative correlation with the thermal aggregation points determined using DLS, showing that more extended species aggregate at lower temperatures.

Structural models of IP_3R_N were refined against the experimental scattering data using the rigid-body refinement program BUNCH,[19] which refines the relative orientation of subunits of known structure against scattering data while accounting for regions of unknown structure. The latter is important, as neglecting the scattering density in regions of unknown structure can bias the derived model. Further, their inclusion provides a useful restraint to constrain the positions of known structural domains such that the interdomain N and C termini are kept within reasonable distances based on the lengths of their linking sequences. In the case of IP_3R_N, the linker region between βI and βII (residues 224–235, designated L-I), absent from the crystal structures of both the suppressor (PDB 1XZZ) and core domains (PDB 1N4K), was included as a linking sequence of unknown structure in BUNCH optimizations. For structures in the presence of IP_3, the IP_3-binding core was kept as a rigid unit, unchanged from the crystal structure. For the structures lacking IP_3, initial BUNCH calculations were performed with a second linking sequence to allow for flexibility between the βII and ARM domains of the IP_3-binding core (residues 435–437, designated L-II). These calculations resulted in models with a variety of open cleft configurations for the IP_3-binding core that fit the data equally well. We therefore treated the IP_3-binding core as a rigid unit in an open configuration for modeling against the data without IP_3, which ensured the number of degrees of freedom modeled for each variant was the same. The calculations for each IP_3R_N variant used all data between $Q=0.02$ Å^{-1} and $Q=0.30$ Å^{-1}, and were repeated ten times to evaluate the uniqueness of the solutions. The solutions obtained for each variant differed with respect to the orientation of the domains, but the set of models for each variant shared common features, most notably with respect to the degree of compactness. The quality of the fit of the models to the

Table 1. Structural parameters derived from the SAXS data

Sample	Protein concentration (mg/ml)	Guinier		$P(r)$	Porod
		R_g (Å)	$I(0)$*	D_{max}	Volume (Å^3)
$IP_3R_N + IP_3$	2.5±0.1	30.7±0.9	0.79±0.05	88	114,500
$IP_3R_N + IP_3 + Ca^{2+}$	2.5±0.1	31.5±0.8	0.82±0.05	95	131,500
IP_3R_N	2.5±0.1	32.6±1.0	0.82±0.05	100	136,500
$IP_3R_N + Ca^{2+}$	2.5±0.1	34.2±1.1	0.85±0.05	110	161,200
Lysozyme	5.5±0.3	14.2±0.3	0.83±0.06	42	n.r.

n.r., not relevant.

experimental data is summarized by the statistical quantity χ^2. The best χ^2 values obtained for each IP_3R_N variant are 1.82 (IP_3R_N), 1.32 ($IP_3R_N + IP_3$), 0.88 ($IP_3R_N + IP_3 + Ca^{2+}$) and 0.81 ($IP_3R_N + Ca^{2+}$), and the corresponding model profiles are superimposed on the experimental scattering data in Figure 5(a). These χ^2 values indicate reasonable fits to the data, though the best results are for the $+Ca^{2+}$ data. The measured scattering profiles represent the time and ensemble average of the conformations present weighted by their relative populations. In a conformationally heterogeneous solution of molecules, the difference between the most compact and extended conformations and the populations of each conformational substate will dictate the quality of the fit of a single model to the measured scattering data. The somewhat poorer fits obtained for the data measured on samples where Ca^{2+} was absent suggests there is a significant population of both compact and extended structures in solution that cannot be modeled adequately by a single structure. The improvement of the fits for data measured on samples where Ca^{2+} is present suggests that this equilibrium is driven such that extended conformations are dominant and can be modeled satisfactorily by a single structure.

Discussion

A major question regarding IP_3R activation is how IP_3 binding to the N-terminal region is translated into a protein conformational change that results in channel opening in a region of the receptor near the C terminus some 2000 amino acid residues away. Many structural analyses have attempted to elucidate the mechanism underlying IP_3R activation, including several recent electron microscopy studies that have provided the 3D structures of IP_3R at low resolution.[9–14] These electron microscopy studies identified two gross conformations of the tetrameric IP_3R complex as viewed from the cytosol.[20] The "square" conformation is assumed to correspond to the closed channel, and the "windmill"-like conformation appears to represent IP_3R in a Ca^{2+}-bound state or possibly even a desensitized Ca^{2+}-free state. We have reported the crystal structures of the suppressor domain and the IP_3-binding core with bound IP_3.[15,16] However, since the structures of these two functional regions were determined as separate polypeptides, little was known about their spatial relationship or the mechanism underlying inhibition of IP_3 binding mediated by the suppressor domain. Here, we have taken a biophysical approach to investigate the domain architecture and ligand-induced conformational changes in the N-terminal region of IP_3R1 (IP_3R_N).

The extensive peak broadening of the ^1H–^{15}N HSQC spectrum of IP_3R_{CORE} without IP_3 bound (Figure 4(b)), essentially disappears upon binding IP_3. Also thermal denaturation (monitored by CD ellipticity at 222 nm) implies that the IP_3-binding core is more stable with bound IP_3 than in the IP_3-free state. Both pieces of evidence suggest IP_3 binding eliminates chemical exchange around L-II (residues 435–437) that links the βII and ARM domains by fixing them into the more rigid L-shaped conformation observed in the crystal structure. This finding is in agreement with recent fluorescent resonance energy transfer (FRET) kinetics studies using the IP_3 sensor IRIS (Venus - $IP_3R_{a.a.\ 224\text{-}575}$–ECFP), which indicate that the IP_3-binding core has at least two conformations in the absence of IP_3.[21] Severe exchange broadening of the ^1H–^{15}N HSQC spectrum of the IP_3-bound IP_3R_N was not caused by protein aggregation, as gel-filtration chromatography and multi-angle light-scattering data confirmed the NMR sample to be a monodisperse monomer (Supplementary Data Figure 5). Comparison of the spectrum at 25 °C (Figure 4(d)) to spectra obtained at 5 °C and 15 °C showed significant changes in linewidths for many of the sharp peaks observed in a ^1H chemical shift range of 7.8 ppm–8.6 ppm (Supplementary Data Figure 4). This severe peak broadening is in agreement with chemical exchange and is less likely due to a change in molecular tumbling time. The time-scale of the chemical shift broadening is in the milli- to microsecond range, consistent with gross movement of globular domains within a protein. Since IP_3 binding should also rigidify the βII and ARM domains in IP_3R_N, it is probable that the extensive broadening observed in this case is due to flexibility in L-I (residues 224–238 connecting βI and βII, i.e. the suppressor domain and IP_3R_{CORE}).

Evidence of conformational variability afforded by the flexible linker L-I can also be deduced from structural modeling against the SAXS data. Our structural modeling indicates that addition of Ca^{2+} results in an increase in the population of more extended conformational states, most likely attributable to L-I allowing the suppressor domain to move

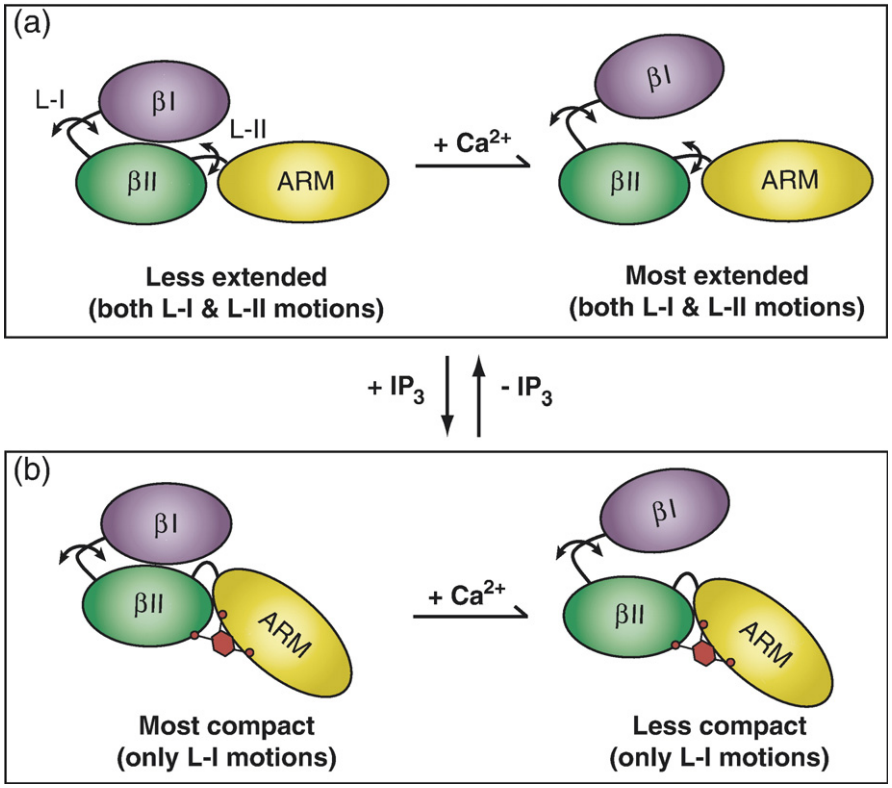

Figure 6. Cartoon representations of IP_3R_N. IP_3R_N exists in multiple ligand-dependent conformational states as mediated by a pair of flexible linkers (L-I and L-II) that join three stably folded domains (β1, βII, and ARM). (a) IP_3-free variants have elongated overall shapes resulting from flexibility in both L-I and L-II linkers. (b) IP_3 (in red) binding restricts L-II motions and compacts the IP_3R_N structure. A lesser and converse effect is observed upon the addition of Ca^{2+}, which drives the equilibrium to favor more extended conformations for both IP_3-bound and IP_3-free variants.

away from the IP_3-binding core (Figure 6). Ca^{2+} is known to act as a co-agonist in IP_3R activation,[3,22] and it is believed that one or more stimulatory Ca^{2+} sites, critical to channel gating, are unmasked by conformational changes that originate from the N-terminal region.[23] Other factors, such as calmodulin[24–26] and CaBP1,[27,28] for example, may also similarly modulate accessibility and/or sampling of the conformational states. We have speculated that there are two Ca^{2+} sites within IP_3R_{CORE}.[16] These putative sites may be responsible for the Ca^{2+} effects observed by the SAXS experiments. However, the Ca^{2+}-binding affinities of these sites appear to be very low, with dissociation constants in the range of 0.1–1 mM (H. P. and J. C., unpublished results), thus raising questions regarding their physiological significance. It was shown recently that mutations at these sites do not affect IP_3R activation,[29] suggesting that further C-terminal high-affinity Ca^{2+}-binding sites, probably involving Glu2100, may be more important for the activation of channel function The concentration of Ca^{2+} within the endoplasmic reticulum lumen ($[Ca^{2+}]_{ER}$) can be as high as 1 mM and, as such, the local cytosolic concentration of Ca^{2+} ($[Ca^{2+}]_c$) in the vicinity of the mouth of the ion pore immediately after channel opening could be much higher than the activated $[Ca^{2+}]_c$ of ~1 μM. It cannot be ruled out that the low-affinity Ca^{2+}-binding sites within IP_3R_N might have an inhibitory role that is physiologically significant after channel opening. While we can only speculate on its regulatory function, Ca^{2+} appears to promote a measurable change in the equilibrium between compact and more extended conformational substates in solutions of IP_3R_N.

The structural modeling against the SAXS data provides evidence of conformational flexibility around L-I, even in the absence of Ca^{2+}. While models that fit the data reasonably well were found for all conditions, those refined against data collected from IP_3R_N solutions in the absence of Ca^{2+} gave statistically poorer fits than those in the presence of Ca^{2+}. We suggest that the poorer fits are due to the fact that we are attempting to model equilibrium mixtures of compact and more extended conformations with a single average structure, and that the differences between the more compact and more extended structures are larger than the differences among the more extended population distributions observed in the presence of Ca^{2+}.

Our data indicate that in the context of the N-terminal region, the suppressor domain interacts with the IP_3-binding core. This finding is supported by the SAXS data modeling, as well as the fact that the suppressor domain has been observed to

contribute to the thermostability of the IP_3-binding core (Figure 3(a) and (b)). Moreover, it is consistent with recent biochemical studies showing that the suppressor domain inhibits IP_3 binding in a manner that requires its covalent linkage to the IP_3-binding core.[30] These observations support the finding that the inhibition of IP_3 binding by the suppressor domain is not simply due to competition with IP_3 or the masking of a preformed IP_3-binding pocket, but rather that L-I is crucial in mediating the proper interaction between the suppressor domain and the IP_3-binding core.

The present study provides new insights into the ligand-induced conformational changes in the N-terminal region of the IP_3 receptor, which is essential for IP_3 binding. While atomic-resolution protein structures provide the ultimate in detail and are necessary for understanding the chemistry of protein function, alternate approaches are needed to characterize and explore the role of flexible regions such as those that link stably folded domains. We have used solution scattering in combination with crystal structure and NMR data to explore the roles of flexible linkers between functional domains in the cAMP-dependent protein kinase.[31–34] The present study on IP_3R_N contributes another example of flexible linker regions that have important roles in inter-domain organization and communication, and thus highlights the importance of combining high-resolution structure determination with methods that can explore the roles of structural flexibility and conformational heterogeneity in biomolecular function.

Materials and Methods

Materials

Trpysin and D-*myo*-inositol 1,4,5-trisphosphate (IP_3) as a hexapotassium salt were purchased from Sigma.

Expression and protein purification

Expression and purification of the IP_3-binding core comprising residues 224–604 of mIP_3R1 (IP_3R_{CORE}) was performed as described.[16] Mouse IP_3R1 residues 1–604 (IP_3R_N) subcloned into the vector pET15b was expressed in *Escherichia coli* BL21-CodonPlus(DE3)-RIL cells (Stratagene) at 15 °C by induction with 0.5 mM IPTG. Cells were harvested 15 h post-induction and lysed by sonication in lysis buffer (15 mM Tris–HCl (pH 8.4), 500 mM NaCl, 20% (v/v) glycerol, 0.2% (v/v) Nonidet P40, 10 mM imidazole, 0.2 mM Tris(2-carboxyethyl)-phosphine (TCEP), 10 mM 2-mercaptoethanol, 10 μg/ml of DNase I, EDTA-free Protease Inhibitor Cocktail tablets (Roche)). The clarified lysate was affinity-purified using Ni-NTA resin (Qiagen) and the eluted protein was subjected simultaneously to thrombin digestion to remove the His_6-tag and dialysis against Tris buffer (15 mM Tris–HCl (pH 8.4), 300 mM NaCl, 0.5 mM TCEP) for ~36 h at 4 °C. The dialyzed sample was applied to a cation-exchange chromatography column (Fractogel EMD SO_3^-; EM Industries Inc.) and eluted with Tris buffer (15 mM Tris-HCl (pH 8.4), 400 mM NaCl, 0.5 mM TCEP). The sample was then further purified by size-exclusion chromatography (Superdex 200; GE Healthcare) in 15 mM Tris–HCl (pH 8.0), 1 mM TCEP. The suppressor domain of IP_3R1 (residues 2–223) was subcloned into the pGEX-2T vector (Amersham Biosciences) and expressed as a glutathione-*S*-transferase-fusion protein (as described above for IP_3R_N). Cells were subjected to sonication in lysis buffer (15 mM Tris–HCl (pH 8.4), 500 mM NaCl, 20% (v/v) glycerol, 0.2% Nonidet P40, 10 mM DTT, 10 μg/ml of DNase I, EDTA-Free Protease Inhibitor Cocktail tablets (Roche)). The clarified lysate was incubated with Glutathione Sepharose 4B (GE Healthcare) resin, washed with washing buffer (15 mM Tris–HCl (pH 8.4), 10% (v/v) glycerol, 300 mM NaCl, 10 mM DTT) and subsequently eluted with the elution buffer (50 mM Tris–HCl (pH 8.4), 10% (v/v) glycerol, 300 mM NaCl, 10 mM DTT, 10 mM glutathione). Thrombin digestion to remove the glutathione-*S*-transferase was carried out simultaneously with dialysis in 20 mM Tris–HCl (pH 8.4), 3% (v/v) glycerol, 300 mM NaCl, 2 mM $CaCl_2$, 0.5 mM TCEP for ~36 h at 4 °C. Finally, size-exclusion chromatography with Superdex 75 (Pharmacia) in 15 mM Tris–HCl (pH 7.1), 3% (v/v) glycerol, 500 mM NaCl, 2 mM TCEP yielded the monomeric form of the protein. ^2H and ^{15}N-labeled proteins were expressed in modified M9 minimal medium supplemented with 1 g/l of [^{15}N]ammonium chloride in 100% ^2H_2O.

Circular dichroism

CD spectra were collected on an AVIV spectrometer model 62DS using a 1 mm path-length cell at 25 °C. Data were collected with an averaging time of 8 s at 0.5 nm resolution with a bandwidth of 1.0 nm. Protein + IP_3 samples contain ~0.3 mM IP_3. Guanidine hydrochloride denaturation of 0.2 mg/ml of IP_3R_N and 0.1 mg/ml of IP_3R_{CORE} was performed in 15 mM Tris–HCl (pH 8.0), 300 mM NaCl, 1 mM TCEP, 5 mM EGTA. Thermal denaturation experiments were recorded under the same buffer conditions at 1 deg.C increments from 25 °C to 80 °C for IP_3R_N, and from 25 °C to 75 °C for IP_3R_{CORE}.

Limited trypsin digestion

Purified IP_3R_N protein at a concentration of 0.6 mg/ml, untreated or in the presence of 5 molar excess IP_3, was incubated with 0.2 μg/ml of trypsin at 37 °C in 15 mM Tris–HCl (pH 8.0), 300 mM NaCl, 1 mM TCEP. The reaction was terminated by the addition of SDS-PAGE sample loading buffer followed by heating to 100 °C for 5 min. Samples were separated by SDS-PAGE (15% (w/v) polyacrylamide gel) and the protein bands were visualized by staining with Coomassie brilliant blue.

Dynamic light-scattering

Dynamic light-scattering experiments were done to evaluate the monodispersity of the protein samples in different ligand-bound states before and after SAXS experiments. The monodispersity of IP_3R_N samples at 20 °C was evaluated using a Dynapro DLS temperature-controlled micro-sampler with a 824.7 nm laser diode (Protein Solutions, Charlottesville, VA). DLS scattering counts were recorded every second (200 acquisitions/sample) and scattering intensity data were processed using Dynamics Dynapro Control software v.6.3.40. IP_3R_N (~2.9 mg/ml) was maintained in 50 mM Tris-

SO_4 (pH 8.8), 100 mM Na_2SO_4, 1 mM $Ca(CH_3COO)_2$, ~14 mM β- mercaptoethanol. Immediately before analysis, individual protein aliquots were supplemented with the following: i, nothing; ii, 2 mM EGTA (pH 8.8); iii, 250 μM IP_3; iv, 2 mM EGTA (pH 8.8) + 250 μM IP_3. The SAXS experiments used these samples as well as samples prepared with 2.5 mg/ml of IP_3R_N in 15 mM Tris–HCl (pH 8.0), 300 mM NaCl, 1 mM TCEP. The SAXS structural parameters derived from both sets of samples showed the same trends. The relative thermal stabilities of the four IP_3R_N variants were determined using DLS essentially as described, except that scattering counts were measured from 7.5–42.5 °C in steps of 2.5 °C.

Small-angle X-ray scattering and modeling

The SAXS data presented in Figure 4 were collected at the Australian Nuclear Science and Technology Organization (ANSTO, Lucas Heights, Australia) on a Bruker Nanostar instrument with a copper target (λ = 1.5418 Å), three-pinhole collimation and HiStar 2D detector with 100 μm pixel size. The 15 μl samples of protein (2.5 mg/ml IP_3R_N in 15 mM Tris–HCl (pH 8.0), 300 mM NaCl, 1 mM TCEP) and matched buffer solutions were mounted sequentially in the same sealed quartz capillary and irradiated for periods of 1 h per exposure at 20 °C. The sample to detector distance was 65 cm, giving a measurable Q range of 0.02–0.34 $Å^{-1}$, where $Q = 4\pi(\sin\theta)/\lambda$, and θ is half the angle between the incident and scattered beams. Exposures for 1 h were acquired for the common buffer, and for the IP_3R_N in each ligand-bound state (no ligand, IP_3, Ca^{2+}, and $IP_3 + Ca^{2+}$). A lysozyme standard was measured so that analysis of $I(0)$ for each of the samples could yield information regarding the association state of the molecules in solution. Data for each exposure were corrected for non-uniform detector response and radially averaged to produce $I(Q)$ *versus* Q profiles using Bruker software. Normalized buffer scattering data were subtracted from the scattering data for the protein solutions using the program PRIMUS in order to obtain the scattering data of the protein alone.[19] Structural parameters for the scattering particle were derived using Guinier analysis,[35] indirect Fourier transform methods (using the program GNOM[17]) and Porod analysis.[18] It is noteworthy that in our SAXS analyses the selection of D_{max} for the calculation of $P(r)$ proved difficult for all IP_3R_N samples. The calculation of $P(r)$ from $I(Q)$ must use indirect Fourier transformation methods due to the fact that data are collected over only a finite measurement range. These methods require an estimate of the maximum dimension of the molecule, D_{max}, which for well-behaved (monodisperse, identical) particles generally may be chosen by simple inspection of the $P(r)$ profile. Selection of D_{max} is more difficult if there is any aggregation or structural heterogeneity in the sample due, for example, to molecular flexibility. In these instances, one can obtain $P(r)$ solutions that appear to be in good agreement with the scattering data, but they give R_g and $I(0)$ values that are significantly larger than those determined by Guinier analysis, and it is difficult to systematically compare $P(r)$ profiles from different samples. We observed this behavior in our IP_3R_N data, and because the DLS and $I(0)$ data preclude aggregation as the cause, it supports our conclusions regarding conformational flexibility. Further evidence of this comes from the fact that the $IP_3R_N + IP_3$ structure, judge to be the least flexible, was the easiest to transform. In order to have a consistent approach to the selection of D_{max} to compare our various IP_3R_N samples, we selected D_{max} values that gave R_g and $I(0)$ values derived from $P(r)$ that agreed with those determined by the Guinier approximation.

Structural modeling against the scattering data was performed using the program BUNCH,[19] which allows the relative dispositions of domains of known atomic structures to be optimized, while including regions of unknown structure in the optimized model. This approach does not yield a high-resolution structure for the unknown structural regions, but does restrain the domains from adopting positions that are physically unreasonable while accounting for the scattering density of the missing parts of a structure.

NMR spectroscopy

NMR buffer conditions for IP_3R_{CORE}, IP_3R_N, and the suppressor domain were as follows: 15 mM Tris–HCl (pH 8.00, 300 mM Na_2SO_4, 2 mM TCEP; 15 mM Tris–HCl (pH 8.0), 300 mM NaCl, 1 mM TCEP; and 15 mM Tris–HCl (pH 7.1), 3% (v/v) glycerol, 300 mM NaCl, 2 mM TCEP, respectively. Purified proteins were concentrated to ~0.7 mM and all NMR experiments were performed at 25 °C (unless indicated otherwise) on a Varian Inova 600 MHz spectrometer and a Bruker Avance III 800 MHz spectrometer equipped with a triple resonance, pulse field gradient probe. Transverse relaxation optimized spectroscopy (TROSY)-based ^1H-^{15}N heteronuclear single quantum coherence (HSQC) data were recorded on the unlabeled IP_3-bound ^2H,^{15}N-labeled IP_3R_{CORE} complexes with 128 and 512 complex points in T_1 and T_2, respectively. The spectral width was 40 ppm for the ^{15}N (F_1) and 15.2 ppm for the ^1H (F_2) dimension, respectively. The apo IP_3R_{CORE} spectrum was recorded with 160 and 512 complex points in T_1 and T_2, respectively. The spectral widths were 35.6 ppm for ^{15}N (F_1) and 16 ppm for ^1H (F_2) dimension, respectively. For the ^2H,^{15}N-suppressor domain, TROSY-based HSQC data were recorded with 128 and 612 complex points in T_1 and T_2, respectively and the spectral width was 26 ppm for ^{15}N (F_1) and 16 ppm (F_2) for the ^1H dimension. TROSY-based HSQC data for IP_3R_N were obtained on a Varian Inova 600 MHz spectrometer equipped with a Varian triple resonance cold probe and data comprised of 128 and 612 complex points in T_1 and T_2, respectively. All NMR data were processed and analyzed using NMRPipe and NMRDraw.[36]

Acknowledgements

We thank M. Plevin for his assistance with NMR data collection and P. Stathopulos for his help with the light-scattering experiments. M.I. is a Canada Research Chair in Cancer Structural Biology. This work was supported, in part, by the Heart and Stroke Foundation of Canada and a CIHR doctoral research award to J.C., was and, in part, by Australian Research Council (ARC) Discovery Project DP0770321 and an ARC Federation Fellowship FF0457488 to J.T. AINSE grant AINGRA06257 (to J.T.) provided access to the X-ray scattering instrument at ANSTO.

Supplementary Data

Supplementary data associated with this article can be found, in the online version, at doi:10.1016/j.jmb.2007.08.057

References

1. Berridge, M. J. (1993). Inositol trisphosphate and calcium signalling. *Nature*, **361**, 315–325.
2. Furuichi, T., Kohda, K., Miyawaki, A. & Mikoshiba, K. (1994). Intracellular channels. *Curr. Opin. Neurobiol.* **4**, 294–303.
3. Finch, E. A., Turner, T. J. & Goldin, S. M. (1991). Calcium as a coagonist of inositol 1,4,5-trisphosphate-induced calcium release. *Science*, **252**, 443–446.
4. Patel, S., Joseph, S. K. & Thomas, A. P. (1999). Molecular properties of inositol 1,4,5-trisphosphate receptors. *Cell Calcium*, **25**, 247–264.
5. Bosanac, I., Michikawa, T., Mikoshiba, K. & Ikura, M. (2004). Structural insights into the regulatory mechanism of IP_3 receptor. *Biochim. Biophys. Acta*, **1742**, 89–102.
6. Yoshikawa, F., Morita, M., Monkawa, T., Michikawa, T., Furuichi, T. & Mikoshiba, K. (1996). Mutational analysis of the ligand binding site of the inositol 1,4,5-trisphosphate receptor. *J. Biol. Chem.* **271**, 18277–18284.
7. Yoshikawa, F., Uchiyama, T., Iwasaki, H., Tomomori-Satoh, C., Tanaka, T., Furuichi, T. & Mikoshiba, K. (1999). High efficient expression of the functional ligand binding site of the inositol 1,4,5-triphosphate receptor in *Escherichia coli*. *Biochem. Biophys. Res. Commun.* **257**, 792–797.
8. Uchida, K., Miyauchi, H., Furuichi, T., Michikawa, T. & Mikoshiba, K. (2003). Critical regions for activation gating of the inositol 1,4,5-trisphosphate receptor. *J. Biol. Chem.* **278**, 16551–16560.
9. Jiang, Q. X., Thrower, E. C., Chester, D. W., Ehrlich, B. E. & Sigworth, F. J. (2002). Three-dimensional structure of the type 1 inositol 1,4,5-trisphosphate receptor at 24 Å resolution. *EMBO J.* **21**, 3575–3581.
10. Hamada, K., Miyata, T., Mayanagi, K., Hirota, J. & Mikoshiba, K. (2002). Two-state conformational changes in inositol 1,4,5-trisphosphate receptor regulated by calcium. *J. Biol. Chem.* **277**, 21115–21118.
11. da Fonseca, P. C., Morris, S. A., Nerou, E. P., Taylor, C. W. & Morris, E. P. (2003). Domain organization of the type 1 inositol 1,4,5-trisphosphate receptor as revealed by single-particle analysis. *Proc. Natl Acad. Sci. USA*, **100**, 3936–3941.
12. Serysheva, I. I., Bare, D. J., Ludtke, S. J., Kettlun, C. S., Chiu, W. & Mignery, G. A. (2003). Structure of the type 1 inositol 1,4,5-trisphosphate receptor revealed by electron cryomicroscopy. *J. Biol. Chem.* **278**, 21319–21322.
13. Hamada, K., Terauchi, A. & Mikoshiba, K. (2003). Three-dimensional rearrangements within inositol 1,4,5-trisphosphate receptor by calcium. *J. Biol. Chem.* **278**, 52881–52889.
14. Sato, C., Hamada, K., Ogura, T., Miyazawa, A., Iwasaki, K., Hiroaki, Y. *et al.* (2004). Inositol 1,4,5-trisphosphate receptor contains multiple cavities and L-shaped ligand-binding domains. *J. Mol. Biol.* **336**, 155–164.
15. Bosanac, I., Yamazaki, H., Matsu-Ura, T., Michikawa, T., Mikoshiba, K. & Ikura, M. (2005). Crystal structure of the ligand binding suppressor domain of type 1 inositol 1,4,5-trisphosphate receptor. *Mol. Cell*, **17**, 193–203.
16. Bosanac, I., Alattia, J. R., Mal, T. K., Chan, J., Talarico, S., Tong, F. K. *et al.* (2002). Structure of the inositol 1,4,5-trisphosphate receptor binding core in complex with its ligand. *Nature*, **420**, 696–700.
17. Svergun, D. I. (1992). Determination of the regularization parameter in indirect-transform methods using perceptual criteria. *J. Appl. Crystallog.* **25**, 495–503.
18. Porod, G. (1951). Die Röntgenkleinwinkelstreuung von dichtgepackten kolloiden Systemen. *Kolloid-Z.* **124**, 83–114.
19. Petoukhov, M. V. & Svergun, D. I. (2005). Global rigid body modeling of macromolecular complexes against small-angle scattering data. *Biophys. J.* **89**, 1237–1250.
20. Taylor, C. W., da Fonseca, P. C. & Morris, E. P. (2004). IP (3) receptors: the search for structure. *Trends Biochem. Sci.* **29**, 210–219.
21. Matsu-ura, T., Michikawa, T., Inoue, T., Miyawaki, A., Yoshida, M. & Mikoshiba, K. (2006). Cytosolic inositol 1,4,5-trisphosphate dynamics during intracellular calcium oscillations in living cells. *J. Cell Biol.* **173**, 755–765.
22. Taylor, C. W. & Laude, A. J. (2002). IP_3 receptors and their regulation by calmodulin and cytosolic Ca^{2+}. *Cell Calcium*, **32**, 321–334.
23. Marchant, J. S. & Taylor, C. W. (1997). Cooperative activation of IP_3 receptors by sequential binding of IP_3 and Ca^{2+} safeguards against spontaneous activity. *Curr. Biol.* **7**, 510–518.
24. Adkins, C. E., Morris, S. A., De Smedt, H., Sienaert, I., Torok, K. & Taylor, C. W. (2000). Ca^{2+}-calmodulin inhibits Ca^{2+} release mediated by type-1, -2 and -3 inositol trisphosphate receptors. *Biochem. J.* **345**, 357–363.
25. Cardy, T. J. & Taylor, C. W. (1998). A novel role for calmodulin: Ca^{2+}-independent inhibition of type-1 inositol trisphosphate receptors. *Biochem. J.* **334**, 447–455.
26. Patel, S., Morris, S. A., Adkins, C. E., O'Beirne, G. & Taylor, C. W. (1997). Ca^{2+}-independent inhibition of inositol trisphosphate receptors by calmodulin: redistribution of calmodulin as a possible means of regulating Ca^{2+} mobilization. *Proc. Natl Acad. Sci. USA*, **94**, 11627–11632.
27. Yang, J., McBride, S., Mak, D. O., Vardi, N., Palczewski, K., Haeseleer, F. & Foskett, J. K. (2002). Identification of a family of calcium sensors as protein ligands of inositol trisphosphate receptor Ca^{2+} release channels. *Proc. Natl Acad. Sci. USA*, **99**, 7711–7716.
28. Kasri, N. N., Holmes, A. M., Bultynck, G., Parys, J. B., Bootman, M. D., Rietdorf, K. *et al.* (2004). Regulation of InsP3 receptor activity by neuronal Ca^{2+}-binding proteins. *EMBO J.* **23**, 312–321.
29. Joseph, S. K., Brownell, S. & Khan, M. T. (2005). Calcium regulation of inositol 1,4,5-trisphosphate receptors. *Cell Calcium*, **38**, 539–546.
30. Iwai, M., Michikawa, T., Bosanac, I., Ikura, M. & Mikoshiba, K. (2007). Molecular basis of the isoform-specific ligand-binding affinity of inositol 1,4,5-trisphosphate receptors. *J. Biol. Chem.* **282**, 12755–12764.
31. Vigil, D., Blumenthal, D. K., Taylor, S. S. & Trewhella, J. (2006). Solution scattering reveals large differences in the global structures of type II protein kinase A isoforms. *J. Mol. Biol.* **357**, 880–889.
32. Vigil, D., Blumenthal, D. K., Taylor, S. S. & Trewhella, J. (2005). The conformationally dynamic C helix of the RIα subunit of protein kinase A mediates isoform-

specific domain reorganization upon C subunit binding. *J. Biol. Chem.* **280**, 35521–35527.
33. Vigil, D., Blumenthal, D. K., Heller, W. T., Brown, S., Canaves, J. M., Taylor, S. S. & Trewhella, J. (2004). Conformational differences among solution structures of the type Iα, IIα and II*β* protein kinase A regulatory subunit homodimers: role of the linker regions. *J. Mol. Biol.* **337**, 1183–1194.
34. Heller, W. T., Vigil, D., Brown, S., Blumenthal, D. K., Taylor, S. S. & Trewhella, J. (2004). C subunits binding to the protein kinase A RIα dimer induce a large conformational change. *J. Biol. Chem.* **279**, 19084–19090.
35. Guinier (1939). La diffraction des rayons X aux tres petits angles; application a l'etude de phenomenes ultramicroscopiques. *Ann. Phys.* **12**, 161–237.
36. Delaglio, F., Grzesiek, S., Vuister, G. W., Zhu, G., Pfeifer, J. & Bax, A. (1995). NMRPipe: a multidimensional spectral processing system based on UNIX pipes. *J. Biomol. NMR*, **6**, 277–293.